# Material barriers to diffusive and stochastic transport

George Haller[a,1], Daniel Karrasch[b], and Florian Kogelbauer[a]

[a]Institute for Mechanical Systems, ETH Zürich, 8092 Zürich, Switzerland; and [b]Zentrum Mathematik, Technische Universität München, 85748 Garching bei München, Germany

Edited by Eric Vanden-Eijnden, Courant Institute of Mathematical Sciences, New York, NY, and accepted by Editorial Board Member Srinivasa S. Varadhan August 2, 2018 (received for review November 19, 2017)

**We seek transport barriers and transport enhancers as material surfaces across which the transport of diffusive tracers is minimal or maximal in a general, unsteady flow. We find that such surfaces are extremizers of a universal, nondimensional transport functional whose leading-order term in the diffusivity can be computed directly from the flow velocity. The most observable (uniform) transport extremizers are explicitly computable as null surfaces of an objective transport tensor. Even in the limit of vanishing diffusivity, these surfaces differ from all previously identified coherent structures for purely advective fluid transport. Our results extend directly to stochastic velocity fields and hence enable transport barrier and enhancer detection under uncertainties.**

diffusive transport | stochastic transport | turbulence | coherent structures | variational calculus

Transport barriers—that is, observed inhibitors of the spread of substances in flows—provide a simplified global template to analyze mixing without testing various initial concentrations and tracking their pointwise evolution in detail. Even though such barriers are well documented in several physical disciplines, including geophysical flows (1), fluid dynamics (2), plasma fusion (3), reactive flows (4), and molecular dynamics (5), no generally applicable theory for their defining properties and detection has emerged. In this paper, we seek to fill this gap by proposing a mathematical theory of transport barriers and enhancers from first principles in the physically ubiquitous regime of small diffusivities (high Péclet numbers).

Diffusive transport is governed by a time-dependent partial differential equation (PDE), whose numerical solution requires knowledge of the initial concentration, the exact diffusivity, and the boundary conditions. Persistently high gradients make this transport PDE challenging to solve accurately for weakly diffusive processes, such as temperature and salinity transport in the ocean and vorticity transport in high-Reynolds number turbulence. That is why one often neglects diffusion and focuses on the purely advective redistribution of the substance, governed by an ordinary differential equation that only involves a deterministic flow velocity field. In that purely advective setting, a transport barrier is often described as a surface with zero material flux. While plausible at first sight, this view actually renders transport barriers grossly ill-defined. Indeed, any codimension-one surface of carrier fluid trajectories (material surface) experiences zero material flux and hence is a barrier by this definition (Fig. 1).

This ambiguity has ignited interest in Lagrangian coherent structures (LCSs, see Fig. 1), which are material surfaces that do not simply block but also organize conservative tracers into coherent patterns (6–9). Due to differing views on finite-time material coherence, however, each available approach yields (mildly or vastly) different structures as LCSs (10). These discrepancies suggest that even purely advective coherent structure detection would benefit from being viewed as the zero-diffusion limit of diffusive barrier detection. Indeed, transport via diffusion through a material surface is a uniquely defined, fundamental physical quantity, whose extremum surfaces can be defined without invoking any special notion of coherence.

A large number of prior approaches to weakly diffusive transport exist, only some of which will be possible to mention here. Among these, spatially localized expansions around simple advective solutions provide appealingly detailed temporal predictions for simple velocity fields (11–13). Writing the advection–diffusion equation in Lagrangian coordinates suggests a quasi-reduction to a one-dimensional diffusion PDE along the most contracting direction, yielding asymptotic scaling laws for stretching and folding statistics along chaotic trajectories (14, 15). Observed transport barriers, however, are not chaotic, and the formal asymptotic expansions used in these subtle arguments remain unjustified. As alternatives, the effective diffusivity approach of ref. 16 and the residual velocity field concept (17) offer attractive visualization tools for regions of enhanced or suppressed transport. Both approaches, however, target already performed diffusive simulations and hence provide descriptive diagnostics rather than prediction tools.

Here we address the diffusive tracer transport problem in its purest, original form. Namely, we seek transport barriers as space-dividing (codimension-one) material surfaces that inhibit diffusive transport more than neighboring surfaces do. Locating material diffusion barriers without simulating diffusion and without reliance on specific initial concentration distributions is the physical problem we define and solve here in precise mathematical terms, assuming only incompressibility and small diffusion. In the limit of vanishing diffusion, our approach also provides a unique, physical definition of LCSs as material surfaces that will block transport most efficiently under the addition of the slightest diffusion or uncertainty to an idealized, purely advective mixing problem. Since the notion of transport through a surface

## Significance

**Observations of tracer transport in fluids generally reveal highly complex patterns shaped by an intricate network of transport barriers and enhancers. The elements of this network appear to be universal for small diffusivities, independent of the tracer and its initial distribution. Here, we develop a mathematical theory for weakly diffusive tracers to predict transport barriers and enhancers solely from the flow velocity, without reliance on diffusive or stochastic simulations. Our results yield a simplified computational scheme for diffusive transport problems, such as the estimation of salinity redistribution for climate studies and the forecasting of oil spill spreads on the ocean surface.**

Author contributions: G.H. and D.K. designed research; G.H. performed research; D.K. and F.K. contributed new numerical/analytical tools; D.K. analyzed data; and G.H. wrote the paper.

The authors declare no conflict of interest.

This article is a PNAS Direct Submission. E.V.-E. is a guest editor invited by the Editorial Board.



[1]To whom correspondence should be addressed. Email: georgehaller@ethz.ch.

This article contains supporting information online at www.pnas.org/lookup/suppl/doi:10.1073/pnas.1720177115/-/DCSupplemental.

Published online August 27, 2018.

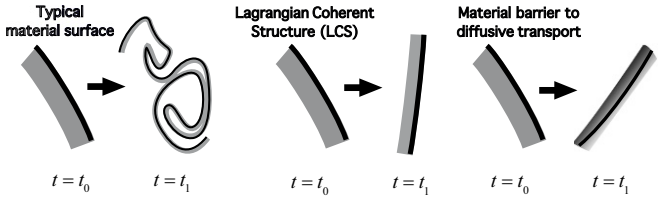


**Fig. 1.** (*Left*) Any material surface is a barrier to advective transport over any time interval $[t_0, t_1]$ but will generally deform into an incoherent shape. (*Middle*) Material surfaces preserving their coherence at their final position at $t_1$ are LCSs. (*Right*) Diffusion barriers, in contrast, are material surfaces minimizing diffusive transport of a concentration field across them over the time interval $[t_0, t_1]$.

is quantitative and universally accepted, this definition of an LCS eliminates the current ambiguity in advective mixing studies, with different approaches identifying different structures as coherent (10).

### Transport Tensor and Transport Functional

The advection–diffusion equation for a tracer $c(\mathbf{x}, t)$ is given by (18)

$$c_t + \boldsymbol{\nabla} \cdot (c\mathbf{v}) = \nu \boldsymbol{\nabla} \cdot (\mathbf{D} \boldsymbol{\nabla} c), \qquad c(\mathbf{x}, t_0) = c_0(\mathbf{x}), \qquad [1]$$

where $\boldsymbol{\nabla}$ denotes the gradient operation with respect to the spatial variable $\mathbf{x} \in U \subset \mathbb{R}^n$ on a compact domain $U$ with $n \geq 1$; $\mathbf{v}(\mathbf{x}, t)$ is an $n$-dimensional, incompressible, smooth velocity field generating the advective transport of $c(\mathbf{x}, t)$ whose initial distribution is $c_0(\mathbf{x})$; $\mathbf{D}(\mathbf{x}, t) = \mathbf{D}^T(\mathbf{x}, t) \in \mathbb{R}^{n \times n}$ is the dimensionless, positive definite diffusion–structure tensor describing possible anisotropy and temporal variation in the diffusive transport of $c$; and $\nu > 0$ is a small diffusivity parameter rendering the full diffusion tensor $\nu\mathbf{D}$ small in norm. We assume that the initial concentration $c(\mathbf{x}, t_0) = c_0(\mathbf{x})$ is of class $C^2$, and the diffusion tensor $\mathbf{D}(\mathbf{x}, t)$ is at least Hölder-continuous, which certainly holds if it is continuously differentiable.

The Lagrangian flow map induced by $\mathbf{v}$ is $\mathbf{F}_{t_0}^t : \mathbf{x}_0 \mapsto \mathbf{x}(t; t_0, \mathbf{x}_0)$, mapping initial material element positions $\mathbf{x}_0 \in U$ to their later positions at time $t$. We assume that trajectories stay in the domain $U$ of known velocities; that is, $\mathbf{F}_{t_0}^t(U) \subset U$ holds for all times $t$ of interest. We will denote by $\boldsymbol{\nabla}_0 \mathbf{F}_{t_0}^t$ the gradient of $\mathbf{F}_{t_0}^t$ with respect to initial positions $\mathbf{x}_0$.

Let $\mathcal{M}(t) = \mathbf{F}_{t_0}^t(\mathcal{M}_0)$ be a time-evolving, $(n-1)$-dimensional material surface in $U$ with boundary $\partial\mathcal{M}(t)$ and with initial position $\mathcal{M}_0 = \mathcal{M}(t_0)$. By construction, the advective flux of $c$ through $\mathcal{M}(t)$ vanishes, and hence, only the diffusive part of the flux vector on the right-hand side of Eq. **1** generates transport through $\mathcal{M}(t)$. The total transport of $c$ through $\mathcal{M}(t)$ over a time interval $[t_0, t_1]$ is therefore given by

$$\Sigma_{t_0}^{t_1} = \int_{t_0}^{t_1} \int_{\mathcal{M}(t)} \nu \mathbf{D} \boldsymbol{\nabla} c \cdot \mathbf{n} \, dA \, dt, \qquad [2]$$

with $dA$ denoting the area element on $\mathcal{M}(t)$ and $\mathbf{n}(\mathbf{x}, t)$ denoting the unit normal to $\mathcal{M}(t)$ at a point $\mathbf{x} \in \mathcal{M}(t)$. Let $dA_0$ and $\mathbf{n}_0(\mathbf{x}_0)$ denote the area element and oriented unit normal vector field on the initial surface $\mathcal{M}(t_0)$. Then, by the classic surface element deformation formula $\mathbf{n} dA = \det\left(\boldsymbol{\nabla}_0 \mathbf{F}_{t_0}^t\right) \left[\boldsymbol{\nabla}_0 \mathbf{F}_{t_0}^t\right]^{-\top} \mathbf{n}_0 dA_0$ (19) and by the chain rule applied to $\boldsymbol{\nabla} c$, we can rewrite the total transport Eq. **2** through $\mathcal{M}(t)$ as

$$\Sigma_{t_0}^{t_1} = \nu \int_{t_0}^{t_1} \int_{\mathcal{M}_0} \left[\boldsymbol{\nabla}_0 c\left(\mathbf{F}_{t_0}^t, t\right)\right]^\top \mathbf{T}_{t_0}^t \mathbf{n}_0 dA_0 \, dt, \qquad [3]$$

with the tensor $\mathbf{T}_{t_0}^t(\mathbf{x}_0) \in \mathbb{R}^{n \times n}$ defined as

$$\mathbf{T}_{t_0}^t = \left[\boldsymbol{\nabla}_0 \mathbf{F}_{t_0}^t\right]^{-1} \mathbf{D}\left(\mathbf{F}_{t_0}^t, t\right) \left[\boldsymbol{\nabla}_0 \mathbf{F}_{t_0}^t\right]^{-\top}. \qquad [4]$$

We note that $\det \mathbf{T}_{t_0}^t = \det\left[\mathbf{D}\left(\mathbf{F}_{t_0}^t, t\right)\right]$ by incompressibility and that

$$\mathbf{T}_{t_0}^t = \left[\mathbf{C}_{t_0}^t\right]^{-1} \qquad [5]$$

holds in case of isotropic diffusion ($\mathbf{D} \equiv \mathbf{I}$), with $\mathbf{C}_{t_0}^t := \left[\boldsymbol{\nabla}_0 \mathbf{F}_{t_0}^t\right]^\top \boldsymbol{\nabla}_0 \mathbf{F}_{t_0}^t$ denoting the right Cauchy–Green strain tensor (19).

As we show in *SI Appendix*, S1, under our assumptions on $\mathbf{v}$ and $\mathbf{D}$, Eq. **3** can be equivalently rewritten as

$$\Sigma_{t_0}^{t_1}(\mathcal{M}_0) = \nu \int_{t_0}^{t_1} \int_{\mathcal{M}_0} \left(\boldsymbol{\nabla}_0 c_0\right)^\top \mathbf{T}_{t_0}^t \mathbf{n}_0 \, dA_0 \, dt + o(\nu), \qquad [6]$$

with the symbol $o(\nu)$ referring to a quantity that, even after division by $\nu$, tends to 0 as $\nu \to 0$. Proving Eq. **6** is subtle, because Eq. **1** is a singularly perturbed PDE for small $\nu > 0$, and hence, its solutions generally cannot be Taylor-expanded at $\nu = 0$, unless $\mathbf{v}$ is integrable (20).

To systematically test the ability of the material surface $\mathcal{M}(t)$ to hinder the transport of $c$ over the time interval $[t_0, t_1]$, we initialize the concentration field $c$ at time $t_0$ locally near $\mathcal{M}_0$ so that $\mathcal{M}_0$ is a level surface of $c_0(\mathbf{x}_0)$ along which $\boldsymbol{\nabla}_0 c_0(\mathbf{x}_0)$ has a constant magnitude $K > 0$. This universal choice of $c_0(\mathbf{x}_0)$ subjects each $\mathcal{M}_0$ surface to the same, most diffusion-prone scalar configuration, ensuring equal detectability for all barriers in our analysis, independent of any specific initial concentration distribution. We can then write $\boldsymbol{\nabla}_0 c_0(\mathbf{x}_0) = K \mathbf{n}_0(\mathbf{x}_0)$, and hence, the total transport in Eq. **6** becomes

$$\Sigma_{t_0}^{t_1}(\mathcal{M}_0) = \nu K (t_1 - t_0) \int_{\mathcal{M}_0} \left\langle \mathbf{n}_0, \bar{\mathbf{T}}_{t_0}^{t_1} \mathbf{n}_0 \right\rangle dA_0 + o(\nu).$$

Here we have introduced the symmetric, positive definite transport tensor $\bar{\mathbf{T}}_{t_0}^{t_1}$ as the time average of $\mathbf{T}_{t_0}^t$ over $t \in [t_0, t_1]$. The same averaged tensor was already proposed heuristically in ref. 11 to simplify the Lagrangian version of Eq. **1**.*

Finally, to give a dimensionless characterization of the transport through the surface $\mathcal{M}(t)$ over the period $[t_0, t_1]$, we normalize $\Sigma_{t_0}^{t_1}(\mathcal{M}_0)$ by the diffusivity $\nu$, by the transport time $(t_1 - t_0)$, by the initial concentration gradient magnitude $K$, and by the surface area $A_0(\mathcal{M}_0)$ (or length, for $n = 2$) of $\mathcal{M}_0$. This leads to the normalized total transport

$$\tilde{\Sigma}_{t_0}^{t_1}(\mathcal{M}_0) := \frac{\Sigma_{t_0}^{t_1}(\mathcal{M}_0)}{\nu K (t_1 - t_0) A_0(\mathcal{M}_0)} = \mathcal{T}_{t_0}^{t_1}(\mathcal{M}_0) + O(\nu^\alpha) \qquad [7]$$

for some $\alpha \in (0, 1)$, where the nondimensional transport functional,

$$\mathcal{T}_{t_0}^{t_1}(\mathcal{M}_0) := \frac{\int_{\mathcal{M}_0} \left\langle \mathbf{n}_0, \bar{\mathbf{T}}_{t_0}^{t_1} \mathbf{n}_0 \right\rangle dA_0}{\int_{\mathcal{M}_0} dA_0}, \qquad [8]$$

is a universal measure of the leading-order diffusive transport through the material surface $\mathcal{M}(t)$ over the period $[t_0, t_1]$. This functional enables a systematic comparison of the quality of transport through different material surfaces. Remarkably, $\mathcal{T}_{t_0}^{t_1}(\mathcal{M}_0)$ can be computed for any initial surface $\mathcal{M}_0$ directly from the trajectories of $\mathbf{v}$, without solving the PDE Eq. **1**. Furthermore, as we show in *SI Appendix*, S2, $\bar{\mathbf{T}}_{t_0}^{t_1}$ and hence $\mathcal{T}_{t_0}^{t_1}$ are objective (frame-indifferent).

*This heuristic simplification generally gives incorrect results for unsteady flows and can only be partially justified for steady flows (12). In our present context, however, $\bar{\mathbf{T}}_{t_0}^{t_1}$ arises without any heuristics.

## General Equation for Diffusive Transport Extremizers

By formula Eq. **7** and by the implicit function theorem, nondegenerate extrema of the normalized total transport $\tilde{\Sigma}_{t_0}^{t_1}$ are $O(\nu^\alpha)$-close to those of the transport functional $\mathcal{T}_{t_0}^{t_1}$, for some $\alpha \in (0,1)$. Initial positions of such transport-extremizing material surfaces are, therefore, necessarily solutions of the variational problem

$$\delta \mathcal{T}_{t_0}^{t_1}(\mathcal{M}_0) = 0, \qquad [9]$$

with boundary conditions yet to be specified, given that the location and geometry of diffusive transport extremizers is unknown at this point. We will refer to minimizers of $\mathcal{T}_{t_0}^{t_1}$ as diffusive transport barriers and to maximizers of $\mathcal{T}_{t_0}^{t_1}$ as diffusive transport enhancers.

Carrying out the variational differentiation in Eq. **9** gives the equivalent extremum problem (cf. ref. 21)

$$\delta \mathcal{E}_{\mathcal{T}_0}(\mathcal{M}_0) = 0, \quad \mathcal{E}_{\mathcal{T}_0}(\mathcal{M}_0) := \int_{\mathcal{M}_0} \left[ \left\langle \mathbf{n}_0, \bar{\mathbf{T}}_{t_0}^{t_1} \mathbf{n}_0 \right\rangle - \mathcal{T}_0 \right] dA_0, \qquad [10]$$

where $\mathcal{T}_0 := \mathcal{T}_{t_0}^{t_1}(\mathcal{M}_0)$ is constant. To transform this problem to a form amenable to classical variational calculus, we need to reformulate Eq. **10** in terms of a (yet unknown) general parameterization $\mathbf{x}_0(s_1, \ldots, s_{n-1})$ of $\mathcal{M}_0$ and then express the integrand in terms of tangent vectors computed from this parametrization. Let $G_{ij}(\partial_{\mathbf{s}}\mathbf{x}_0(\mathbf{s})) = \left\langle \frac{\partial x_0}{\partial s_i}, \frac{\partial x_0}{\partial s_j} \right\rangle$, $i,j = 1, \ldots, n-1$ denotes the $(i,j)$ entry of the Gramian matrix $\mathbf{G}(\partial_{\mathbf{s}}\mathbf{x}_0(\mathbf{s}))$ of the parametrization. As we show in *SI Appendix*, S3, after reparametrization and passage from normal to tangent vectors in the integrand, we can rewrite the functional $\mathcal{E}_{\mathcal{T}_0}$ in Eq. **10** in the form

$$\mathcal{E}_{\mathcal{T}_0}(\mathcal{M}_0) = \int_{\mathcal{M}_0} L\left(\mathbf{x}_0(\mathbf{s}), \partial_{\mathbf{s}}\mathbf{x}_0(\mathbf{s})\right) ds_1 \ldots ds_{n-1}, \qquad [11]$$

with the Lagrangian

$$L(\mathbf{x}_0, \partial_{\mathbf{s}}\mathbf{x}_0) = \frac{\det \bar{\mathbf{T}}_{t_0}^{t_1}(\mathbf{x}_0) \det \left[ \mathbf{G}\left( \left( \bar{\mathbf{T}}_{t_0}^{t_1}(\mathbf{x}_0) \right)^{-\frac{1}{2}} \partial_{\mathbf{s}}\mathbf{x}_0 \right) \right]}{\sqrt{\det \mathbf{G}(\partial_{\mathbf{s}}\mathbf{x}_0)}} - \mathcal{T}_0 \sqrt{\det \mathbf{G}(\partial_{\mathbf{s}}\mathbf{x}_0)}. \qquad [12]$$

The Euler–Lagrange equations associated with the Lagrangian Eq. **12** are given by the $n$-dimensional set of coupled nonlinear, second-order PDEs

$$\frac{\partial L}{\partial \mathbf{x}_0} - \sum_{i=1}^{n-1} \frac{\partial}{\partial s_i} \frac{\partial L}{\partial (\partial_{s_i}\mathbf{x}_0)} = \mathbf{0}. \qquad [13]$$

## Uniform Extremizers of Diffusive Transport

Eq. **13** has infinitely many solutions through any point $\mathbf{x}_0$ of the physical space, yet most of these solution surfaces remain unobserved as significant barriers due to large variations in the concentration gradient along them. Most observable are transport extremizers that maintain a nearly uniform drop in the scalar concentration along them, implying that the transport density along them is as uniform as possible.

As we show in *SI Appendix*, S4, even perfectly uniform extremizers of $\mathcal{T}_{t_0}^{t_1}$ exist and form the zero-level set $\{L = 0\}$ in the phase space of Eq. **13**. As we see from Eq. **12**, these uniform transport extremizer solutions of Eq. **13** satisfy the first-order family of PDEs,

$$\det \bar{\mathbf{T}}_{t_0}^{t_1} \det \left[ \mathbf{G}\left( \left( \bar{\mathbf{T}}_{t_0}^{t_1} \right)^{-\frac{1}{2}} \partial_{\mathbf{s}}\mathbf{x}_0 \right) \right] = \mathcal{T}_0 \det \left[ \mathbf{G}(\partial_{\mathbf{s}}\mathbf{x}_0) \right], \qquad [14]$$

for any choice of the parameter $\mathcal{T}_0 > 0$. Note that, by construction, $\mathcal{T}_0$ then equals to the uniform diffusive transport density across any subset of the material surface $\mathcal{M}(t)$ over the time interval $[t_0, t_1]$.

An equivalent form of Eq. **14** follows from the observation that the functional $\mathcal{E}_{\mathcal{T}_0}$ is invariant under reparametrizations, and hence $\mathcal{L}_0$ can also be computed from the original, surface normal-based form Eq. **10** of the underlying variational principle. The latter form simply gives $\left\langle \mathbf{n}_0, \bar{\mathbf{T}}_{t_0}^{t_1} \mathbf{n}_0 \right\rangle = \mathcal{T}_0$ on $\mathcal{L}_0$, which we further rewrite as

$$\left\langle \mathbf{n}_0(\mathbf{x}_0), \mathbf{E}_{\mathcal{T}_0}(\mathbf{x}_0) \mathbf{n}_0(\mathbf{x}_0) \right\rangle = 0, \qquad \mathbf{E}_{\mathcal{T}_0} := \bar{\mathbf{T}}_{t_0}^{t_1} - \mathcal{T}_0 \mathbf{I}. \qquad [15]$$

This reveals that diffusive transport extremizers are null-surfaces of the metric tensor $\mathbf{E}_{\mathcal{T}_0}(\mathbf{x}_0)$—that is, their normals have zero length in the metric defined by $\mathbf{E}_{\mathcal{T}_0}(\mathbf{x}_0)$.

For such null surfaces to exist through a point $\mathbf{x}_0$, the metric generated by $\mathbf{E}_{\mathcal{T}_0}$ must have null directions. This limits the domain of existence of transport extremizers with uniform transport density $\mathcal{T}_0$ to spatial domains where the eigenvalues $0 < \lambda_1(\mathbf{x}_0) \leq \ldots \leq \lambda_n(\mathbf{x}_0)$ of the positive definite tensor $\bar{\mathbf{T}}_{t_0}^{t_1}(\mathbf{x}_0)$ satisfy $\lambda_1(\mathbf{x}_0) \leq \mathcal{T}_0 \leq \lambda_n(\mathbf{x}_0)$.

Finding computable sufficient conditions for the solutions of the variational problem in Eq. **10** to be minimizers does not appear to be within reach. Effective necessary conditions, however, can help greatly in identifying null surfaces of $\mathbf{E}_{\mathcal{T}_0}(\mathbf{x}_0)$ that are likely candidates for extremizers. One such necessary condition requires the trace of the tensor $\mathbf{E}_{\mathcal{T}_0}$ to be nonnegative, as we show in *SI Appendix*, S5. This enables us to summarize our main results for transport extremizers in the following theorem.

**Theorem 1.** A uniform minimizer $\mathcal{M}_0$ of the transport functional $\mathcal{T}_{t_0}^{t_1}$ is necessarily a nonnegatively traced null surface of the tensor field $\mathbf{E}_{\mathcal{T}_0}$—that is,

$$\left\langle \mathbf{n}_0(\mathbf{x}_0), \mathbf{E}_{\mathcal{T}_0}(\mathbf{x}_0) \mathbf{n}_0(\mathbf{x}_0) \right\rangle = 0, \qquad \operatorname{trace} \mathbf{E}_{\mathcal{T}_0}(\mathbf{x}_0) \geq 0, \qquad [16]$$

holds at every point $\mathbf{x}_0 \in \mathcal{M}_0$ with unit normal $\mathbf{n}_0(\mathbf{x}_0)$ to $\mathcal{M}_0$. Similarly, a uniform maximizer $\mathcal{M}_0$ of $\mathcal{T}_{t_0}^{t_1}$ is necessarily a nonpositively traced null surface of the tensor field $\mathbf{E}_{\mathcal{T}_0}$—that is,

$$\left\langle \mathbf{n}_0(\mathbf{x}_0), \mathbf{E}_{\mathcal{T}_0}(\mathbf{x}_0) \mathbf{n}_0(\mathbf{x}_0) \right\rangle = 0, \qquad \operatorname{trace} \mathbf{E}_{\mathcal{T}_0}(\mathbf{x}_0) \leq 0, \qquad [17]$$

holds at every point $\mathbf{x}_0 \in \mathcal{M}_0$.

***Remark 1:*** Assume that the flow is 2D ($n = 2$) and the diffusion is homogeneous and isotropic ($\mathbf{D} = \mathbf{I}$). Then, replacing the averaged transport tensor $\bar{\mathbf{T}}_{t_0}^{t_1}$ with its unaveraged counterpart $\mathbf{T}_{t_0}^{t_1}$ in our arguments, we obtain that closed material curves that extremize the diffusive flux uniformly at $t = t_1$ coincide with 2D elliptic Lagrangian coherent structures (LCSs) (22). Similarly, replacing $\bar{\mathbf{T}}_{t_0}^{t_1}$ with the transport-rate tensor $\dot{\mathbf{T}}_{t_0}^{t_0} := -\left[ \nabla \mathbf{v} + [\nabla \mathbf{v}]^T \right]$,[†] the flux rate at $t = t_0$ coincides with elliptic objective Eulerian coherent structures (OECSs) (23).

Remark 1 connects instantaneous flux and flux-rate extremizing surfaces under homogeneous and isotropic diffusion to LCSs and EOCSs. In the $\nu \to 0$ limit, however, material diffusion barriers identified by Theorem 1 differ from advective coherent structures identified in previous studies (cf. *SI Appendix*, S7). While this conclusion is at odds with the usual assumptions of purely advective transport studies, it is mathematically consistent with the singular perturbation nature of the diffusion term in Eq. **1**.

[†] Note that $\dot{\mathbf{T}}_{t_0}^{t_0} = -2\mathbf{S}$, where $\mathbf{S}$ is the classic rate-of-strain tensor for the velocity field $\mathbf{v}$. we obtain that closed curves that uniformly extremize the diffusive.

***Remark 2:*** As seen in the proof of Theorem 1 in *SI Appendix*, S5, $\operatorname{trace}\mathbf{E}_{\mathcal{T}_0}(\mathbf{x}_0)=\operatorname{trace}\bar{\mathbf{T}}^{t_1}_{t_0}(\mathbf{x}_0)-n\mathcal{T}_0$ measures how strongly the normalized transport changes from $\mathcal{T}_0$ under localized normal perturbations at $\mathbf{x}_0$ to a transport extremizer $\mathcal{M}_0$. Consequently, the Diffusion Barrier Strength (DBS), defined as

$$\mathrm{DBS}(\mathbf{x}_0):=\operatorname{trace}\bar{\mathbf{T}}^{t_1}_{t_0}(\mathbf{x}_0) \qquad [18]$$

serves as an objective diagnostic scalar field that highlights centerpieces of regions filled with the most influential transport extremizers. Specifically, the time $t_0$ positions of the most prevailing diffusion barriers should be marked approximately by ridges of $\mathrm{DBS}(\mathbf{x}_0)$ field, while the time $t_0$ positions of the least prevailing diffusion barriers should be close to trenches of $\mathrm{DBS}(\mathbf{x}_0)$. A similar conclusion holds for diffusion enhancers based on features of the $\mathrm{DBS}(\mathbf{x}_0)$ field computed in backward time.

By Remark 2, features of the scalar field $\mathrm{DBS}(\mathbf{x}_0)$ play a role analogous to that of the finite-time Lyapunov exponents (FTLEs) in purely advective transport (7). Unlike the FTLE field, however, $\mathrm{DBS}(\mathbf{x}_0)$ is a predictive diagnostic (i.e., requires no diffusive simulation) and arises directly from the technical construction of diffusion extremizers (rather than being one possible indicator of their anticipated properties). Still, $\mathrm{DBS}(\mathbf{x}_0)$ is a visual diagnostic, while Theorem 1 provides the exact equations that diffusion barriers and enhancers satisfy.

## Application to 2D Flows

Here we solve the general barrier–enhancer equations Eqs. **16** and **17** explicitly for 2D flows and write out a more specific form of the diagnostic $\mathrm{DBS}(\mathbf{x}_0)$ for such flows. In two dimensions ($n=2$), a one-dimensional transport extremizer curve $\mathbf{x}_0(s)$ is parametrized by a single scalar parameter $s\in\mathbb{R}^1$. As we show in *SI Appendix*, S6, the Lagrangian $L$ in Eq. **12** then simplifies to

$$L(\mathbf{x}_0,\mathbf{x}_0')=\frac{\langle\mathbf{x}_0',\bar{\mathbf{C}}_{\mathbf{D}}(\mathbf{x}_0)\mathbf{x}_0'\rangle}{\sqrt{\langle\mathbf{x}_0',\mathbf{x}_0'\rangle}}-\mathcal{T}_0\sqrt{\langle\mathbf{x}_0',\mathbf{x}_0'\rangle}, \qquad [19]$$

with the tensor field

$$\bar{\mathbf{C}}_{\mathbf{D}}:=\frac{1}{t_1-t_0}\int_{t_0}^{t_1}\det\left[\mathbf{D}\left(\mathbf{F}^t_{t_0},t\right)\right]\left[\mathbf{T}^t_{t_0}\right]^{-1}dt \qquad [20]$$

denoting the time-averaged, diffusivity structure-weighted version of the classic right Cauchy–Green strain tensor $\mathbf{C}^t_{t_0}$ introduced in Eq. **5**. The Euler–Lagrange Eq. **13** now forms a four-dimensional system of ODEs, which we write out for reference in *SI Appendix*, S6. Uniform transport barriers and enhancers lie in the set $\mathcal{L}_0=\{L=0\}$ in the $(\mathbf{x}_0,\mathbf{x}_0')$ phase space of this ODE. Equating Eq. **19** with zero, we obtain that solutions in $\mathcal{L}_0$ satisfy $\langle\mathbf{x}_0',(\bar{\mathbf{C}}_{\mathbf{D}}(\mathbf{x}_0)-\mathcal{T}_0\mathbf{I})\mathbf{x}_0'\rangle=0$ and hence are precisely the null-geodesics of the one-parameter family of tensors

$$\hat{\mathbf{E}}_{\mathcal{T}_0}(\mathbf{x}_0)=\bar{\mathbf{C}}_{\mathbf{D}}(\mathbf{x}_0)-\mathcal{T}_0\mathbf{I}, \qquad [21]$$

which are Lorentzian (i.e., indefinite) metric tensors on the spatial domain satisfying $\lambda_1(\mathbf{x}_0)<\mathcal{T}_0<\lambda_2(\mathbf{x}_0)$. This extends the mathematical analogy pointed out in refs. 22 and 24 between coherent vortex boundaries and photon spheres around black holes from advective to diffusive mixing. In this analogy, the role of the relativistic metric tensor on the four-dimensional spacetime is replaced by the tensor $\hat{\mathbf{E}}_{\mathcal{T}_0}(\mathbf{x}_0)$ on the 2D physical space of initial conditions.

We seek unit tangent vectors to null-geodesics of $\hat{\mathbf{E}}_{\mathcal{T}_0}$ as a linear combination $\mathbf{x}_0'=\boldsymbol{\eta}_{\mathcal{T}_0}(\mathbf{x}_0)=\alpha\boldsymbol{\xi}_1\pm\sqrt{1-\alpha^2}\boldsymbol{\xi}_2$ of the unit eigenvectors $\boldsymbol{\xi}_i(\mathbf{x}_0)$ corresponding to the eigenvalues $0<\lambda_1(\mathbf{x}_0)\le\lambda_2(\mathbf{x}_0)$ of the positive definite tensor $\bar{\mathbf{C}}_{\mathbf{D}}(\mathbf{x}_0)$. Substituting this linear combination into $\langle\mathbf{x}_0',(\bar{\mathbf{C}}_{\mathbf{D}}(\mathbf{x}_0)-\mathcal{T}_0\mathbf{I})\mathbf{x}_0'\rangle=0$ and solving for $\alpha\in[0,1]$ gives the direction field family

$$\mathbf{x}_0'=\boldsymbol{\eta}_{\mathcal{T}_0}(\mathbf{x}_0):=\sqrt{\tfrac{\lambda_2-\mathcal{T}_0}{\lambda_2-\lambda_1}}\boldsymbol{\xi}_1\pm\sqrt{\tfrac{\mathcal{T}_0-\lambda_1}{\lambda_2-\lambda_1}}\boldsymbol{\xi}_2 \qquad [22]$$

for null-geodesics of $\hat{\mathbf{E}}_{\mathcal{T}_0}$, defined only on the domain where $\lambda_1(\mathbf{x}_0)\le\mathcal{T}_0\le\lambda_2(\mathbf{x}_0)$. Trajectories of $\boldsymbol{\eta}_{\mathcal{T}_0}$ experience uniform pointwise transport density $\mathcal{T}_0$ over the time interval $[t_0,t_1]$. For homogeneous, isotropic diffusion ($\mathbf{D}\equiv\mathbf{I}$), we have $\bar{\mathbf{T}}^{t_1}_{t_0}=\bar{\mathbf{C}}^{-1}_{\mathbf{D}}$ by incompressibility (cf. *SI Appendix*, S6). Consequently, the scalar diagnostic featured in Remark 2 takes the specific form $\mathrm{DBS}(\mathbf{x}_0)=\lambda_1(\mathbf{x}_0)+\lambda_2(\mathbf{x}_0)$. Finally, as we show in *SI Appendix*, S6, there are only three types of robust barriers to diffusion in 2D flows: fronts, jet cores, and families of closed material curves forming material vortices. This is consistent with observations of large-scale geophysical flows (1).

## Particle Transport Extremizers in Stochastic Velocity Fields

Here, we show how our results on barriers to diffusive scalar transport carry over to probabilistic transport barriers to fluid particle motion with uncertainties. Such motions are typically modeled by diffusive Itô processes of the form

$$d\mathbf{x}(t)=\mathbf{v}(\mathbf{x}(t),t)\,dt+\sqrt{\nu}\mathbf{B}(\mathbf{x}(t),t)\,d\mathbf{W}(t), \qquad [23]$$

where $\mathbf{x}(t)\in\mathbb{R}^n$ is the random position vector of a particle at time $t$; $\mathbf{v}(\mathbf{x},t)$ denotes the incompressible, deterministic drift in the particle motion; and $\mathbf{W}(t)$ is an $m$-dimensional Wiener process with diffusion matrix $\sqrt{\nu}\mathbf{B}(\mathbf{x},t)\in\mathbb{R}^{n\times m}$. Here the dimensionless, nonsingular diffusion structure matrix $\mathbf{B}$ is $\mathcal{O}(1)$ with respect to the small parameter $\nu>0$.

Let $p(\mathbf{x},t;\mathbf{x}_0,t_0)$ denote the probability density function (PDF) for the current particle position $\mathbf{x}(t)$ with initial condition $\mathbf{x}_0(t_0)=\mathbf{x}_0$. This PDF is known to satisfy the classic Fokker–Planck equation (25)

$$p_t+\boldsymbol{\nabla}\cdot(p\mathbf{v})=\nu\tfrac{1}{2}\boldsymbol{\nabla}\cdot\left[\boldsymbol{\nabla}\cdot\left(\mathbf{B}\mathbf{B}^\top p\right)\right]. \qquad [24]$$

We can rewrite Eq. **24** as

$$p_t+\boldsymbol{\nabla}\cdot(p\tilde{\mathbf{v}})=\nu\boldsymbol{\nabla}\cdot\left(\tfrac{1}{2}\mathbf{B}\mathbf{B}^\top\boldsymbol{\nabla}p\right),\quad \tilde{\mathbf{v}}=\mathbf{v}-\tfrac{\nu}{2}\boldsymbol{\nabla}\cdot\left(\mathbf{B}\mathbf{B}^\top\right), \qquad [25]$$

which is of advection–diffusion form, Eq. **1**, if $\tilde{\mathbf{v}}$ is incompressible—that is, if

$$\boldsymbol{\nabla}\cdot\left[\boldsymbol{\nabla}\cdot\left(\mathbf{B}(\mathbf{x},t)\mathbf{B}^\top(\mathbf{x},t)\right)\right]\equiv 0. \qquad [26]$$

Assuming Eq. **26** (which holds, e.g., for homogeneous diffusion), we define the probabilistic transport tensor $\bar{\mathbf{P}}^{t_1}_{t_0}$ as the time average of

$$\mathbf{P}^{t_1}_{t_0}:=\frac{1}{2}\left[\boldsymbol{\nabla}_0\mathbf{F}^t_{t_0}\right]^{-1}\mathbf{B}\left(\mathbf{F}^t_{t_0},t\right)\mathbf{B}^\top\left(\mathbf{F}^t_{t_0},t\right)\left[\boldsymbol{\nabla}_0\mathbf{F}^t_{t_0}\right]^{-\top}.$$

We then conclude that all our results on diffusive scalar transport in a deterministic velocity field carry over automatically to particle transport in the stochastic velocity field Eq. **23** with the substitution $\bar{\mathbf{T}}^{t_1}_{t_0}=\bar{\mathbf{P}}^{t_1}_{t_0}$. Namely, we have the following:

**Theorem 2.** With the substitution $\mathbf{E}_{\mathcal{T}_0}(\mathbf{x}_0)=\bar{\mathbf{P}}^{t_1}_{t_0}-\mathcal{T}_0\mathbf{I}$ and under assumption Eq. **26**, uniform barriers and enhancers to the transport of the probability-density $p(\mathbf{x},t_1;\mathbf{x}_0,t_0)$ in the stochastic velocity field Eq. **23** are null surfaces satisfying Theorem 1.

This result enables a purely deterministic computation of observed surfaces of particle accumulation and particle clearance without a Monte Carlo simulation for Eq. **23**.

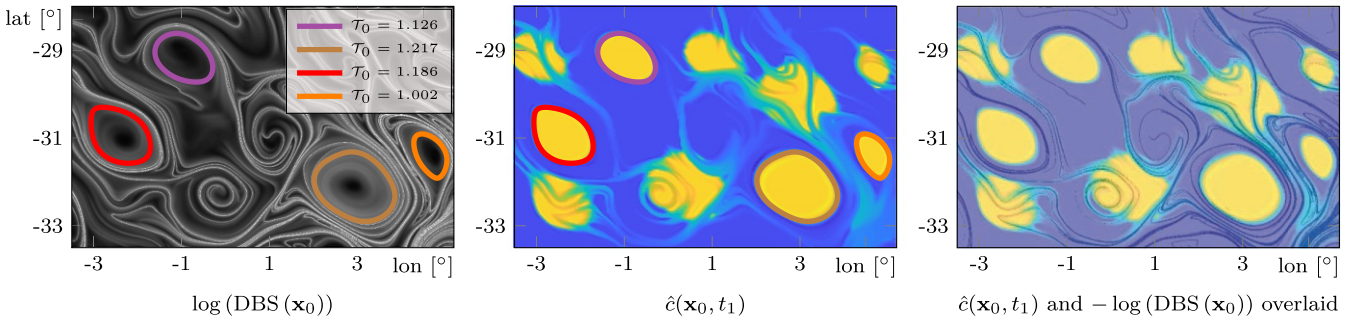


**Fig. 2.** (*Left*) Predicted closed diffusion barriers overlaid on the log(DBS($\mathbf{x}_0$)) field; lighter colors mark higher DBS values. (*Middle*) The diffused concentration, $\hat{c}(\mathbf{x}_0, t_1) := c(\mathbf{F}_{t_0}^{t_1}(\mathbf{x}_0), t_1)$, in Lagrangian coordinates $\mathbf{x}_0$; lighter colors mark higher concentration values; see also Movie S1. The initial concentration $c_0(\mathbf{x}_0)$ is equal to 1 inside the predicted closed barriers and inside seven shifted copies thereof (cf. Fig. 3) and to 0 outside. (*Right*) The ridges of log(DBS) overlaid on $\hat{c}(\mathbf{x}_0, t_1)$.

## Numerical Implementation and Example

For a 2D velocity field $\mathbf{v}(\mathbf{x}, t)$ and diffusion–structure tensor $\mathbf{D}(\mathbf{x}, t)$, the main algorithmic steps in locating diffusion barriers over a time interval $[t_0, t_1]$ are as follows (cf. *SI Appendix*, S7 for more detail and a simple example):

*A1*) Define a Lagrangian grid $\mathcal{G}_0$ of initial conditions; generate trajectories $\mathbf{x}(t, t_0, \mathbf{x}_0)$ of the velocity field $\mathbf{v}(\mathbf{x}, t)$ with initial conditions $\mathbf{x}_0 \in \mathcal{G}_0$ at time $t_0$.

*A2*) For all times $t \in [t_0, t_1]$, compute the deformation gradient $\nabla_0 \mathbf{F}_{t_0}^t(\mathbf{x}_0) = \nabla_0 \mathbf{x}(t, t_0, \mathbf{x}_0)$ over the grid $\mathcal{G}_0$ by finite differencing in $\mathbf{x}_0$ (cf. ref. 7). Then, compute the tensor field $\bar{\mathbf{C}}_\mathbf{D}$ in Eq. **20**.

*A3*) Compute the diffusion–barrier strength diagnostic $\mathrm{DBS}(\mathbf{x}_0) = \mathrm{trace}\,\bar{\mathbf{C}}_\mathbf{D}(\mathbf{x}_0)$. Its ridges and trenches highlight the most influential diffusion barriers (backward-time fronts and jet cores, respectively) at time $t_0$.

*A4*) Compute eigenvalues $\lambda_1(\mathbf{x}_0)$, $\lambda_2(\mathbf{x}_0)$, and corresponding eigenvectors $\boldsymbol{\xi}_1(\mathbf{x}_0)$, $\boldsymbol{\xi}_2(\mathbf{x}_0)$ of $\bar{\mathbf{C}}_\mathbf{D}(\mathbf{x}_0)$. Compute closed diffusion barriers as limit cycles of Eq. **22**. Outermost members of the limit-cycle families mark diffusion-based material vortex boundaries at time $t_0$.

*A5*) To locate time-$t$ positions of material diffusion barriers, advect them using the flow map $\mathbf{F}_{t_0}^t$.

For probabilistic diffusion barriers in the stochastic velocity field Eq. **23**, apply steps A1–A5 after setting $\mathbf{D} = \frac{1}{2}\mathbf{B}\mathbf{B}^\top$.

Our main example will illustrate steps A1–A5 in the identification of boundaries for the largest mesoscale eddies in the Southern Ocean. Known as Agulhas rings, theses eddies are believed to contribute significantly to global circulation and climate via the warm and salty water they ought to carry (26). Several studies have sought to estimate material transport via these eddies by determining their boundaries from different material coherence principles, which all tend to give different results (22, 27–30). Here, we locate the boundaries of Agulhas rings based on the very principle that makes them significant: their role as universal barriers to the diffusion of relevant ocean water attributes they transport.

Fig. 2 shows diffusive coherent Agulhas ring boundaries and surrounding diffusive barriers (backward-time fronts) in the Southern Ocean, computed via steps A1–A5 from satellite altimetry-based surface velocities (cf. *SI Appendix*, S7 for more detail on the dataset). The predicted material ring boundaries are obtained as described in step A4. This prediction is confirmed by a diffusion simulation with Péclet number $Pe = \mathcal{O}(10^4)$; see also the Eulerian analogue in *SI Appendix*, Fig. S4 of the diffused concentration in Movie S1. Fig. 2, *Right* also confirms a similar barrier role for the ridges of $\mathrm{DBS}(\mathbf{x}_0)$, which closely align with observed open barriers to diffusive transport.

Fig. 3 shows the final result of a Monte Carlo simulation of Eq. **23** in the Lagrangian frame (cf. *SI Appendix*, S7), given by

$$d\mathbf{x}_0(t) = \sqrt{\nu}\mathbf{B}_0(\mathbf{x}_0(t), t)\,d\mathbf{W}(t), \mathbf{B}_0 := \left[\nabla_0 \mathbf{F}_{t_0}^t\right]^{-1}\mathbf{B}\left(\mathbf{F}_{t_0}^t, t\right),$$

with homogeneous diffusion–structure matrix $\mathbf{B} = \mathbf{I}$, whose Fokker–Planck equation coincides with the advection–diffusion equation in our previous simulation. The figure confirms the role of the ring boundaries (computed from the deterministic velocity field) as sharp barriers to particle transport under uncertainties in the velocity field. We show the evolving Monte Carlo simulation in Movies S1 and S2.

## Conclusions

We have pointed out that the presence of the slightest diffusion in a deterministic flow yields an unambiguous, first principles-based physical definition for transport barriers as material surfaces that block diffusive transport the most efficiently. We have found that in any dimension, such barriers lie close to minimizers of a universal, nondimensionalized transport functional that measures the leading-order diffusive transport through material surfaces. Of these minimizers, a special set of most observable barriers is formed by those that maintain uniformly high-concentration gradients, and hence uniform transport density, along themselves. Even such uniform barriers, however, will generally differ from coherent structures identified from purely advective considerations (Remark 1). Beyond the exact

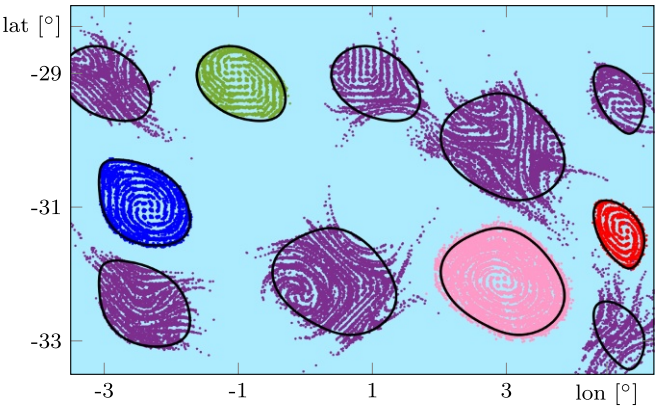


**Fig. 3.** Final positions of stochastic trajectories in the Lagrangian frame (cf. Eq. **7**), initialized from the interiors of the closed black lines: blue, green, pink, and red are initialized within the closed diffusion barriers; purple ones are released from their translated copies for direct comparison. See Movie S2 for the full animation in the Lagrangian frame and Movie S3 in the physical (Eulerian) frame.

differential equations describing transport barriers, we have obtained a predictive diagnostic field, $\mathrm{DBS}(\mathbf{x}_0)$, that signals diffusion barrier location and strength from purely advective computations (Remark 2). Finally, we have discussed how the proposed methodology identifies probabilistic material barriers and enhancers to particle transport in multidimensional stochastic velocity fields.

Our results identify the main enhancers and inhibitors of transport in diffusive and random flows without costly numerical solutions of PDEs or Monte Carlo simulations of stochastic flow models. By construction, the structures we obtain are robust with respect to small diffusive effects, including measurement uncertainties in observational velocity data or modeling errors in numerically generated velocity fields. Our detection scheme for transport extremizers is independent of the local availability of the diffusive tracer and of the initial distribution of its gradient field. The theoretically optimal transport extremizers identified here should also be useful as benchmarks for the development for future diagnostics targeting transport barriers in sparse data. Further theoretical work is required for a more detailed classification of diffusion extremizers in higher dimensions and in compressible flows. On the computational side, the accurate identification of diffusion extremizers identified here requires efficient numerical schemes for null-surfaces. On the applications side, further examples of practically relevant and multiscale velocity fields need to be analyzed in detail to assess further practical implications of the barrier-detection method introduced here.

**ACKNOWLEDGMENTS.** We are grateful to R. Abernathey, F. J. Beron-Vera, T. Breunung, S. Katsanoulis, A. Constantin, M. Mathur, G. Pavliotis, M. Rubin, and J.- L. Thiffeault for useful discussions and comments, and to N. Schilling for contributions to the animation code. G.H. and D.K. acknowledge support from the Turbulent Superstructures priority program of the German National Science Foundation (DFG).

1. Weiss JB, Provenzale A (2008) *Transport and Mixing in Geophysical Flows* (Springer, Berlin).
2. Ottino JM (1989) *The Kinematics of Mixing: Stretching, Chaos and Transport* (Cambridge Univ Press, Cambridge).
3. Dinklage A, Klinger T, Marx G, Schweikhard L (2005) *Plasma Physics—Confinement, Transport and Collective Effects* (Springer, Heidelberg).
4. Rosner D (2000) *Transport Processes in Chemically Reacting Flow Systems* (Butterworth Publishers, Boston).
5. Toda M, Komatsuzaki T, Konishi T, Berry RS, Rice SA, eds (2005) *Geometrical Structures of Phase Space in Multi-Dimensional Chaos: Applications to Chemical Reaction Dynamics in Complex Systems* (Wiley, Hoboken, NJ).
6. Peacock T, Dabiri J (2010) Focus issue on Lagrangian coherent structures. *Chaos* 20:017501.
7. Haller G (2015) Lagrangian coherent structures. *Annu Rev Fluid Mech* 47:137–162.
8. Bahsoun W, Bose C, Froyland G (2014) *Ergodic Theory, Open Dynamics, and Coherent Structures* (Springer, New York).
9. Peacock T, Froyland G, Haller G (2015) Focus issue on the objective detection of coherent structures. *Chaos* 25:087201.
10. Hadjighasem A, Farazmand M, Blazevski D, Froyland G, Haller G (2017) A critical comparison of Lagrangian methods for coherent structure detection. *Chaos* 27:053104.
11. Press WH, Rybicki GB (1981) Enhancement of passive diffusion and suppression of heat flux in a fluid with time-varying shear. *Astrophys J* 248:751–766.
12. Knobloch E, Merryfield WJ (1992) Enhancement of diffusive transport in oscillatory flows. *Astrophys J* 401:196–205.
13. Thiffeault J-L (2008) Scalar decay in chaotic mixing. *Lect Notes Phys* 744:3–35.
14. Tang XZ, Boozer AH (1996) Finite time Lyapunov exponent and advection-diffusion equation. *Physica D* 95:283–305.
15. Thiffeault J-L (2003) Advection-diffusion in Lagrangian coordinates. *Phys Lett A* 30:415–422.
16. Nakamura N (2008) Quantifying inhomogeneous, instantaneous, irreversible transport using passive tracer field as a coordinate. *Lect Notes Phys* 744:137–144.
17. Pratt L, Barkan R, Rypina I (2016) Scalar flux kinematics. *Fluids* 1:27.
18. Landau LD, Lifshitz EM (1966) *Fluid Mechanics* (Pergamon, Oxford).
19. Gurtin ME, Fried E, Anand L (2010) *The Mechanics and Thermodynamics of Continua* (Cambridge Univ Press, Cambridge, UK).
20. Liu W, Haller G (2004) Strange eigenmodes and decay of variance in the mixing of diffusive tracers. *Physica D* 188:1–39.
21. Castillo E, Luceno A, Pedregal P (2008) Composition functionals in calculus of variations. Application to products and quotients. *Math Models Methods Appl Sci* 18:47–75.
22. Haller G, Beron-Vera FJ (2013) Coherent Lagrangian vortices: The black holes of turbulence. *J Fluid Mech* 731:R4.
23. Serra M, Haller G (2016) Objective Eulerian coherent structures. *Chaos* 26:053110.
24. Haller G, Beron-Vera FJ (2014) Addendum to 'Coherent Lagrangian vortices: The black holes of turbulence'. *J Fluid Mech* 755:R3.
25. Risken H (1984) *The Fokker-Planck Equation: Methods of Solution and Applications* (Springer, New York).
26. Beal LM, De Ruijter WPM, Biastoch A, Zahn R (2011) On the role of the Agulhas system in ocean circulation and climate. *Nature* 472:429–436.
27. Froyland G, Horenkamp C, Rossi V, van Sebille E (2015) Studying an Agulhas ring's long-term pathway and decay with finite-time coherent sets. *Chaos* 25: 083119.
28. Hadjighasem A, Haller G (2016) Level set formulation of two-dimensional Lagrangian vortex detection methods. *Chaos* 26:103102.
29. Wang Y, Beron-Vera FJ, Olascoaga MJ (2016) The life cycle of a coherent Lagrangian Agulhas ring. *J Geophys Res [Oceans]* 121:3944–3954.
30. Haller G, Hadjighasem A, Farazmand M, Huhn F (2016) Defining coherent vortices objectively from the vorticity. *J Fluid Mech* 795:136–173.